Electrodeposited Sb and Sb/Sb_2O_3 Nanoparticle Coatings as Anode Materials for Li-Ion Batteries

Hanna Bryngelsson, Jonas Eskhult, Leif Nyholm,* Merja Herranen, Oscar Alm, and Kristina Edström

Department of Materials Chemistry, The Ångström Laboratory, Uppsala University, P.O. Box 538, SE-751 21 Uppsala, Sweden

Received October 17, 2006. Revised Manuscript Received December 21, 2006

Galvanostatically electrodeposited coatings of pure Sb or co-deposited Sb and Sb_2O_3 nanoparticles, prepared from antimony tartrate solutions, were studied as anode materials in Li-ion batteries. It is demonstrated that the co-deposition of 20−25% (w/w) Sb_2O_3 results from a local pH increase at the cathode (due to protonation of liberated tartrate) in poorly buffered solutions. This causes precipitation of Sb_2O_3 nanoparticles and inclusion of some of the particles in the deposit where they become coated with a protecting layer of Sb. Chronopotentiometric cycling of the deposits, which also were characterized using, e.g., SEM, TEM, and XRD, clearly showed that the Sb_2O_3-containing deposits were superior as anode materials. While the Sb/Sb_2O_3 coatings exhibited a specific capacity close to the Sb theoretical value of 660 $mA{\cdot}h{\cdot}g^{-1}$ during more than 50 cycles, the capacity for the Sb coatings gradually decreased to about 250 $mA{\cdot}h{\cdot}g^{-1}$. This indicates that the influence of the significant volume changes present upon the formation and oxidation of Li_3Sb was much smaller for the Sb/Sb_2O_3 nanoparticle coatings. The improved performance can be explained by significant formation of Sb_2O_3 during the reoxidation, the presence of smaller Sb particles in the Sb/Sb_2O_3 coatings, and the formation of buffering nanoparticles of Li_2O in a matrix of Sb during the first reduction cycle for the Sb/Sb_2O_3 deposits.

1. Introduction

The Li-ion battery is well-established on the market and continual studies are made to improve its performance. Graphite is the most commonly used anode material today but efforts are made to find new anode materials with enhanced capacities and improved rate capabilities. There is currently considerable interest in metal-based anode materials (involving elements such as Sb, Sn, Si, and Al) because of their high Li-storage capacities.[1,2] The large volume expansion of these anode materials during the lithiation process is, however, a severe problem. This volume change leads to particle loss and pulverization of the anode material, which drastically limits the cycle life. Different approaches have been described to overcome this problem. Glass matrixes have been studied in which the glass network acts as a buffer for the volume changes.[3,4] The use of nanoalloys,[5,6] active and inactive composite alloy materials, and intermetallic compounds (such as Cu_2Sb,[7] InSb,[8,9] SnSb,[10,11] and AlSb[9,12]) can likewise be employed to circumvent the problem. This type of intermetallic compound (A_xB_y) has a strong structural relationship with its lithiated products and reacts with Li^+ through a fully reversible displacement process, during which the metallic A element is extruded from the structure during the discharge, but readmitted upon charging. Another approach involves the manufacturing of nanostructured electrodes for which the effects of the volume expansion have been reported to be decreased.[13,14] The use of transition metal oxides as anodes involves lithium conversion reactions consisting of an electrochemically driven reversible decomposition of the oxide precursor (MO) electrode into an M/Li_2O nanocomposite electrode that can release Li^+ upon the following charge.[15,16] These $M^{n+} \rightarrow M^0$ conversion reactions can

* Corresponding author. Tel.: +46 (0)18 4713742. Fax: +46 (0)18 513548. Leif.Nyholm@mkem.uu.se.

(1) Besenhard, J. O. *Handbook of Battery Materials*; Wiley-VCH: Weinheim, 1999.
(2) Tarascon, J.-M.; Armand, M. *Nature* **2001**, *414*, 359.
(3) Courtney, I. A.; Dahn, J. R. *J. Electrochem. Soc.* **1997**, *144*, 2045.
(4) Gejke, C.; Zanghellini, E.; Börjesson, L.; Fransson, L.; Edström, K. *J. Phys. Chem. Solids* **2001**, *62*, 1213.
(5) Yang, J.; Winter, M.; Besenhard, J. O. *Solid State Ionics* **1996**, *90*, 281.
(6) Li, H.; Shi, L.; Wang, Q.; Chen, L.; Huang, X. *Solid State Ionics* **2002**, *148*, 247.
(7) Fransson, L.; Vaughey, J. T.; Benedek, R.; Edström, K.; Thomas, J. O.; Thackeray, M. M. *Electrochem. Commun.* **2001**, *3*, 317.
(8) Johnson, C. S.; Vaughey, J. T.; Thackeray, M. M.; Sarakonsri, T.; Hackney, S. A.; Fransson, L.; Edström, K.; Thomas, J. O. *Electrochem. Commun.* **2000**, *2*, 595.
(9) Vaughey, J. T.; Johnson, C. S.; Kropf, A. J.; Benedek, R.; Thackeray, M. M.; Tostmann, H.; Sarakonsri, T.; Hackney, S.; Fransson, L.; Edström, K.; Thomas, J. O. *J. Power Sources* **2001**, *97−98*, 194.
(10) Trifonova, A.; Wachtler, M.; Winter, M.; Besenhard, J. O. *Ionics* **2002**, *8*, 321.
(11) Mukaibo, H.; Osaka, T.; Reale, P.; Panero, S.; Scrosati, B.; Wachtler, M. *J. Power Sources* **2004**, *132*, 225.
(12) Honda, H.; Sakaguchi, H.; Fukuda, Y.; Esaka, T. *Mater. Res. Bull.* **2003**, *38*, 647.
(13) Li, N.; Martin, C. R.; Scrosati, B. *J. Power Sources* **2001**, *97−98*, 240.
(14) Li, N.; Martin, C. R.; Scrosati, B. *Electrochem. Solid-State Lett.* **2000**, *3*, 316.
(15) Poizot, P.; Laruelle, S.; Grugeon, S.; Dupont, L.; Tarascon, J.-M. *Nature* **2000**, *407*, 496.
(16) Armand, M.; Dalard, F.; Deroo, D.; Mouliom, C. *Solid State Ionics* **1985**, *15*, 205.

10.1021/cm0624769 CCC: $37.00
Published on Web 02/08/2007

involve as many as $2e^-$ (CoO) or $4e^-$ (RuO_2) per formula unit as compared to only one for classical insertion/deinsertion reactions.[15,16]

In this study, coatings composed of electrodeposited Sb and Sb/Sb_2O_3 have been studied as anode materials for Li-ion batteries. Sb compounds exhibit high capabilities of storing Li and have therefore been proposed as potential anode materials for Li-ion batteries[7−12,17−19] despite the toxicity of Sb compounds. During the reduction of Sb, a compound containing three Li atoms can be formed,[20] as shown in reaction (1) below:

$$3Li^+ + 3e^- + Sb \leftrightarrow Li_3Sb \quad (1)$$

The latter reaction corresponds to a theoretical capacity of 660 mA·h·g^{-1}, which may be compared to 372 mA·h·g^{-1} for graphite. The expected volume expansion (ca. 150%[21]) during the lithiation process, however, generally leads to a dramatic capacity loss during cycling of this type of material.[20] One possibility to minimize this capacity loss could be to use thin coatings composed of a mixture of Sb and Sb_2O_3 which are reduced to a Sb/Li_2O nanocomposite upon the first cycle, as has previously been described for many 3d metal (Co, Ni, Fe, Cu, and Mn) based oxides.[15,16] Such Sb/Sb_2O_3 materials should be possible to electrodeposit using a similar approach as that described[22−26] for the manufacturing of Cu/Cu_2O coatings. In a recent report, Xue and Fu[27] demonstrated the reversible formation and decomposition of Li_2O for crystalline Sb_2O_3 thin films also containing about 14 mol % Sb. It was demonstrated that the coatings exhibited a high reversible capacity between 691 and 794 mA·h·g^{-1} with good cycling stability. A large irreversible capacity loss (234 mA·h·g^{-1}) was, however, seen on the first cycle.

While Pralong et al.[19] recently studied nanometer thin cobalt antimonide and antimony films prepared by pulsed laser deposition and Xue and Fu[27] employed similarly obtained Sb_2O_3 coatings, we are interested in comparing the properties of electrodeposited Sb and Sb/Sb_2O_3 coatings. Electrodeposition is an inexpensive and straightforward method which generally is carried out at low temperature. The technique facilitates large-scale production of coatings which makes it interesting for industrial applications. As electrodeposition also offers precise control of the deposition reactions, by controlling either the potential or the current density, the structure, phase composition, and thickness of the deposited coatings can likewise be controlled. An additional advantage of using electrodeposition is that the anode materials can be directly deposited on a metallic substrate later serving as the current collector. In these cases, there is hence no need for the use of additional components such as binders and electron-conducting materials (e.g., carbon black), the presence of which may make the interpretation of the results more complex. The absence of binders etc. naturally also leads to a higher density of the active material in the anode materials.

Although a number of reports on the electrodeposition of antimony can be found in the literature,[26,28−35] the possibility of carrying out co-deposition of Sb and Sb_2O_3 by use of a local pH increase has to our knowledge not been investigated previously. The corresponding co-deposition of copper and Cu_2O from lactate, tartrate, or citrate solutions has, however, been described.[22−25] In the latter cases, it has been found[24,25] that Cu_2O is formed as a result of the local pH increase caused by the protonation of the ligand released from the copper(II) complexes upon their reduction. If antimony is electrodeposited from a solution containing antimony tartrate, it is reasonable to assume that a corresponding local pH effect should be present, which could result in a co-deposition of Sb and Sb_2O_3. Such co-depositions were most likely obtained already by Ghosh and Kappana[26] who studied the electrodeposition of antimony from tartrate baths in the presence and absence of hydrochloric acid. The latter authors noted that black deposits were obtained upon deposition from a tartrate solution in the absence of added acid while brilliant white deposits were found after adding HCl (or another acid) to the electrolyte. The compositions of the deposits were, however, not investigated. Ghosh and Kappana[26] also found that the quality of the deposit was improved when the acid strength and/or the quantity of the acid was increased. Increased current densities were, on the other hand, found to result in inhomogeneous black and spongy deposits.

The aim of the present work is to electrodeposit and characterize coatings of Sb and Sb/Sb_2O_3, respectively, and to study the electrochemical behavior of these coatings, particularly the influence of the presence of Sb_2O_3 in the coatings on the electrochemical behavior of the materials when used as anodes in Li-ion batteries. Since the limited cycle life has been found to be the main problem for Sb-based anode materials, our main interest is the cycle stability and the general electrochemical performance of the anode materials in the presence and absence of Sb_2O_3. The influence of the electrolyte composition used in the electrodeposition

(17) Ionica, C. M.; Aldon, L.; Lippens, P. E.; Morato, F.; Olivier-Fourcade, J.; Jumas, J.-C. *Hyperfine Interact.* **2004**, *156/157*, 555.
(18) Tarascon, J.-M.; Morcrette, M.; Dupont, L.; Chabre, Y.; Payen, C.; Larcher, D.; Pralong, V. *J. Electrochem. Soc.* **2003**, *150*, A732.
(19) Pralong, V.; Leriche, J.-B.; Beaudoin, B.; Naudin, E.; Morcrette, M.; Tarascon, J.-M. *Solid State Ionics* **2004**, *166*, 295.
(20) Tirado, J. L. *Mater. Sci. Eng.* **2003**, *R40*, 103.
(21) Besenhard, J. O.; Hess, M.; Komenda, P. *Solid State Ionics* **1990**, *40−41*, 525.
(22) Golden, T. D.; Shumsky, M. G.; Zhou, Y.; VanderWerf, R. A.; Van Leeuwen, R. A.; Switzer, J. A. *Chem. Mater.* **1996**, *8*, 2499.
(23) Leopold, S.; Herranen, M.; Carlsson, J.-O. *J. Electrochem. Soc.* **2001**, *148*, C513.
(24) Leopold, S.; Herranen, M.; Carlsson, J.-O.; Nyholm, L. *J. Electroanal. Chem.* **2003**, *547*, 45.
(25) Eskhult, J.; Herranen, M.; Nyholm, L. *J. Electroanal. Chem.* **2006**, *594*, 35.
(26) Ghosh, J. C.; Kappana, A. N. *J. Phys. Chem.* **1924**, *28*, 149.
(27) Xue, M.-Z.; Fu, Z.-W. *Electrochem. Commun.* **2006**, *8*, 1250.
(28) Past, V. In *Encyclopedia of Electrochemistry of the Elements*; Bard, A. J., Ed.; Marcel Dekker: New York, 1975; Vol. IV, Chapter IV-I.
(29) Sadana, Y. N.; Singh, J. P.; Kumar, R. *Surf. Techn.* **1985**, *24*, 319.
(30) Paolucci, F.; Mengoli, G.; Musiani, M. M. *J. Appl. Electrochem.* **1990**, *20*, 868.
(31) Jung, C.; Rhee, C. K. *J. Electroanal. Chem.* **2004**, *566*, 1.
(32) Yan, J. W.; Wu, Q.; Shang, W. H.; Mao, B. W. *Electrochem. Commun.* **2004**, *6*, 843.
(33) Hara, M.; Inukai, J.; Yoshimoto, S.; Itaya, K. *J. Phys. Chem.* **2004**, *108*, 17441.
(34) Ward, L. C.; Stickney, J. L. *Phys. Chem. Chem. Phys.* **2001**, *3*, 3364.
(35) Yang, M.-H.; Sun, I.-W. *J. Appl. Electrochem.* **2003**, *33*, 1077.

step on the morphology and composition of the coatings is discussed based on scanning electron microscopy (SEM), transmission electron microscopy (TEM), X-ray diffraction (XRD), photoelectron spectroscopy (XPS), and Raman spectroscopic investigations. The electrodeposition reactions and possible reasons for the influence of the Sb_2O_3 content on the electrochemical performance of the anode materials are also discussed.

2. Experimental Section

2.1. Electrodeposition. The electrodeposition was carried out using mainly two electrolytes with different pH but with the same concentration of Sb(III). The first electrolyte had a pH of 1.3 and contained 0.075 M potassium antimony tartrate trihydrate ($K_2(Sb_2(C_4H_2O_6)_2)\cdot 3H_2O$, Fluka, reagent grade) as well as 0.090 M KCl (Merck, pro analysi) and 0.110 M HCl (Fluka, Purum). The pH of the second electrolyte, containing only 0.075 M potassium antimony tartrate trihydrate dissolved in deionized water, was 4.1. In the depositions, pieces of Ni foil (Goodfellow, thickness 0.0125 mm, purity level 99.9%) were used as working electrodes. A platinum wire served as the counter electrode while a saturated calomel electrode (SCE) was used as the reference electrode. A laboratory-designed combined sample holder and electrochemical cell consisting of a polyvinyl chloride (PVC) cylinder, in which the Ni foil served as the bottom section, was used during the electrodepositions. The Ni foil was placed on a 3 mm thick copper plate, used as the current collector, on top of a 10 mm thick PVC plate. The area of the working electrode, and hence the electrodeposited material, was 31.2 cm^2. From this original sample, smaller samples with an area of 3.14 cm^2 were punched out for electrochemical characterization. The electrodepositions were performed at 23 °C in quiescent solution using a constant cathodic current density of either 1.94 or 4.0 mA/cm^2, unless stated otherwise. The experiments were performed with an EG&G model 273 potentiostat/galvanostat (EG&G Princeton Applied Research, Princeton, New Jersey).

Two different pretreatment approaches were used to clean the surface of the Ni substrate prior to the depositions. In the first approach, the nickel foil was etched with 4 M HNO_3 at 40 °C, mainly to facilitate the electrodeposition of Sb on the Ni electrodes. In the second approach, the Ni electrodes were instead cleaned in acetone for 15 min in an ultrasonic bath. After both pretreatments, and prior to the electrodepositions, the Ni substrates were rinsed with deionized water.

The electrodepositions in the presence of 0.110 M HCl were carried out for 100 s using a current density of 4.0 mA/cm^2 on both the HNO_3-etched Ni electrodes and the Ni electrodes cleaned in acetone. In the electrolyte not containing HCl, the latter deposition parameters were also used for the etched Ni electrodes while a current density of 1.94 mA/cm^2 for 120 s was used for the Ni electrodes cleaned in acetone.

2.2. Characterization of the Electrodeposits. The morphology of the coatings was studied with a scanning electron microscope (LEO 1550) while the composition and structure of the deposits were investigated using X-ray diffraction (T2T Siemens D5000 diffractometer with Cu Kα radiation). Transmission electron microscopy (TEM) micrographs of powders scratched off from the deposited coatings were also obtained using a JEOL 2000 FXII instrument. The Sb_2O_3 was identified with Raman spectroscopy employing a Renishaw 2000 Raman spectrometer equipped with a near-infrared diode laser (783 nm, 20 mW). The Raman measurements were also made on scratched off powder. X-ray photoelectron spectroscopy (XPS) was used to examine the oxidation state of the antimony in the coatings prepared in the presence and absence of HCl, respectively. These experiments were performed with a PHI 5500 system using monochromatic Al Kα (1486.6 eV) radiation.

To enable calculations of the specific capacity of the coatings used as the anode materials, it is crucial to determine the mass of active material of the electrode. Since the masses of the samples used for the electrochemical characterization (which had an area of 3.14 cm^2) were too small (i.e., of the order of 0.5 mg) to weigh reliably, these masses were instead calculated from the mass of the deposited larger sample (which had an area of 31.2 cm^2) assuming uniform electrodeposition.

The mass increase of the working electrode during the electrodeposition experiments was also studied with the electrochemical quartz crystal microbalance (EQCM) technique. In these experiments, the electrodeposited masses were compared with those obtained as a result of the bulk depositions onto the Ni-foil electrodes. In the EQCM experiments, 9 MHz AT-cut gold-coated quartz crystals (Seiko EG&G model QA-A9M-Au-50) were utilized as working electrodes. Prior to the antimony electrodepositions, the gold-coated quartz crystals were coated with a 45 nm thick layer of metallic nickel by electrodeposition from a 0.4 Ni(II) (sulfate), 0.8 M tartrate solution (pH 6.1) at a potential of −1.1 V vs SCE during 100 s. A PTFE dip cell holder was used to mount the quartz crystals to expose only one side of the crystal to the deposition solution. The changes in the frequency were monitored with a quartz crystal analyzer (SEIKO EG&G model QCA 922) and data were sampled under computer control employing WinEchem (EG&G). The gate time was set to 0.1 s.

2.3. Electrochemical Characterization of the Coatings. Prior to the cell preparation, the electrodeposited coatings were cut into circular electrodes ($A = 3.14$ cm^2) and dried at 120 °C overnight in a vacuum furnace in an argon-filled glovebox (<3 ppm H_2O and O_2). The typical mass of the active material was 0.5 mg for the Sb deposits and 0.4 mg for the Sb_2O_3-containing deposits. The electrolyte used in the characterization experiments was 1 M $LiPF_6$ dissolved in a 2:1 solution of ethyl carbonate (EC):diethyl carbonate (DEC) (Merck, battery grade). The $LiPF_6$ salt was dried at 80 °C under vacuum overnight prior to use. The water content of the electrolyte was found to be <10 ppm by Karl Fischer titration. The electrochemical test cells, which were manufactured in the argon-filled glovebox, consisted of a stack of the working electrode, a 38 μm thick glass-wool separator soaked in electrolyte, and a lithium foil counter electrode which was vacuum-packed in a polymer-coated aluminum package with attached nickel contacts. In addition to the cells described above, a cell containing a large electrode (31.2 cm^2) was also made using a Sb_2O_3 containing coating. The specific capacity of the latter large electrode cell was compared with those based on the smaller electrodes to ensure that the calculated masses of the smaller electrodes were reliable. The electrochemical performance of the electrodes was studied by cycling the cells between 1.5 and 0.01 V vs Li^+/Li for 50 cycles at a C/10 rate (implying 10 h for a complete lithiation of the electrode material) using a Digatron BTS-600 system. The rate capability of the cells was also studied by galvanostatic cycling between 1.5 and 0.01 V (vs Li^+/Li) at four different rates: C/10 for eight cycles followed by C/6 for four cycles; C/3 for four cycles; C for four cycles; and finally C/10 for four cycles. The latter tests were also carried out with the Digatron BTS-600 system.

3. Results and Discussion

3.1. Electrodeposition and Characterization of the Sb and Sb/Sb_2O_3 Coatings. The electrodeposition experiments in the presence and absence of HCl resulted in coatings with

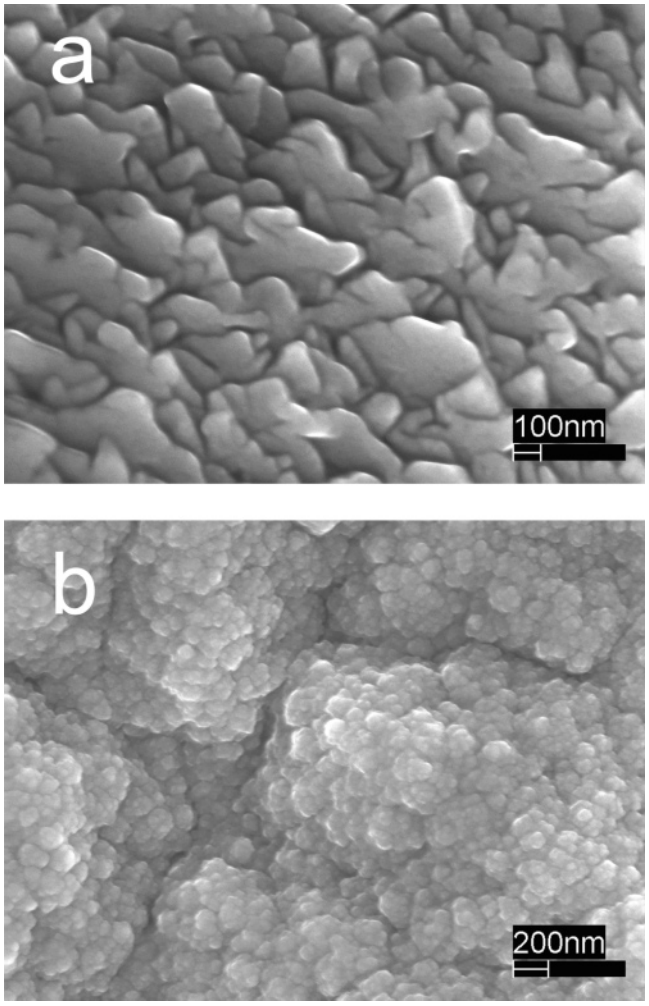

Figure 1. Scanning electron micrograph on (a) a pure Sb coating deposited in the presence of 0.110 M HCl with a cathodic current density of 4.0 mA/cm^2 for 100 s and (b) an Sb_2O_3-containing coating deposited in the absence of HCl using a cathodic current density of 1.92 mA/cm^2 for 120 s.

significantly different appearances in agreement with the results described by Ghosh and Kappana.[26] When the electrodeposition was performed in the electrolyte containing HCl, it was difficult to obtain uniform deposits unless the Ni electrodes were previously etched with HNO_3. On the etched Ni electrodes, brittle and silvery white coatings with large well-defined crystals (see Figure 1a) were, on the other hand, obtained. The fact that uniform coatings could not be obtained on the Ni electrodes only cleaned in acetone in an ultrasonic bath indicates that nucleation problems were present during the latter depositions. These problems were, however, significantly smaller when the depositions were performed in the absence of HCl. In the latter case, black and smooth uniform deposits, which were composed of agglomerated particles (see Figure 1b), were obtained on both the etched and acetone-cleaned Ni electrodes. There was thus no significant influence of the electrode pretreatment on the morphology of the coatings when the depositions were performed in the absence of HCl. The present results, which clearly show that different deposits are obtained in the presence and absence of 0.110 M HCl, indicate that the nucleation is more difficult in the presence of HCl in the electrolyte (i.e., at a pH of 1.3). The SEM micrographs in

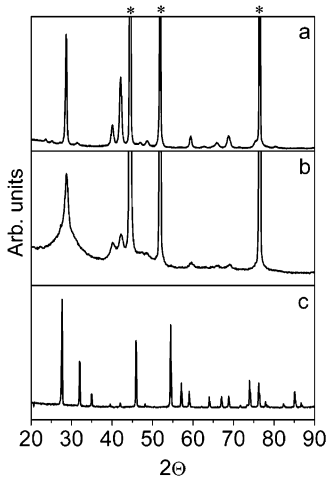

Figure 2. X-ray diffraction patterns obtained for (a) a pure Sb coating, (b) an Sb/Sb_2O_3 coating, and (c) Sb_2O_3 precipitated from the electrolyte by additions of NaOH. The * symbols denote Ni substrate peaks. All other peaks in (a) and (b) are due to Sb while all peaks in (c) are due to Sb_2O_3.

Figure 1 also indicate that smaller particles were obtained in the absence than in the presence of HCl. If not stated otherwise, all coatings prepared in the presence of HCl discussed below were deposited on Ni substrate etched in HNO_3 while the depositions in the absence of HCl were made on Ni substrates only cleaned in acetone.

To study the composition of the deposits obtained during the electrodepositions, the coatings were first analyzed by XRD. As is seen in Figure 2, significantly different XRD patterns were found for the deposits prepared in the presence and absence of HCl. The XRD pattern for the deposit obtained in the presence of HCl (see Figure 2a) only exhibits peaks typical for antimony. Although the peak at 28.7° in 2θ is much broader in Figure 2b, only Sb peaks are likewise seen in the pattern for the deposit obtained in the absence of HCl. There are hence no peaks in Figure 2b that can be definitely ascribed to crystalline Sb_2O_3. A close examination of the broad peak at 28.7° in 2θ reveals that this peak may in fact be explained by a broad Sb (012) peak superimposed on a sharper (012) Sb peak. Based on this assumption, the crystallite sizes were estimated to be approximately 95 and 16 nm, respectively, using Scherrer's equation. This consequently suggests that the Sb/Sb_2O_3 deposit contained two different Sb crystallite sizes. A corresponding evaluation of the Sb peak at 28.6° in 2θ in Figure 2a resulted in a crystallite size of 260 nm, in reasonable agreement with the SEM results in Figure 1a.

Since it was suspected that Sb_2O_3 could form during the electrodeposition in the absence of HCl due to a result of a local pH increase in the vicinity of the working electrode, an experiment was also made in which sodium hydroxide was added to the electrolyte not containing HCl. It was observed that the additions of hydroxide gave rise to the formation of a precipitate, the diffraction pattern of which (see Figure 2c) was found to be identical to that for cubic Sb_2O_3, senarmontite (JCPSD card no. 71-0365), for pH values larger than about 6. This demonstrates that precipitation of Sb_2O_3 can take place if the local pH at the electrode is increased sufficiently during the electrodeposition. A

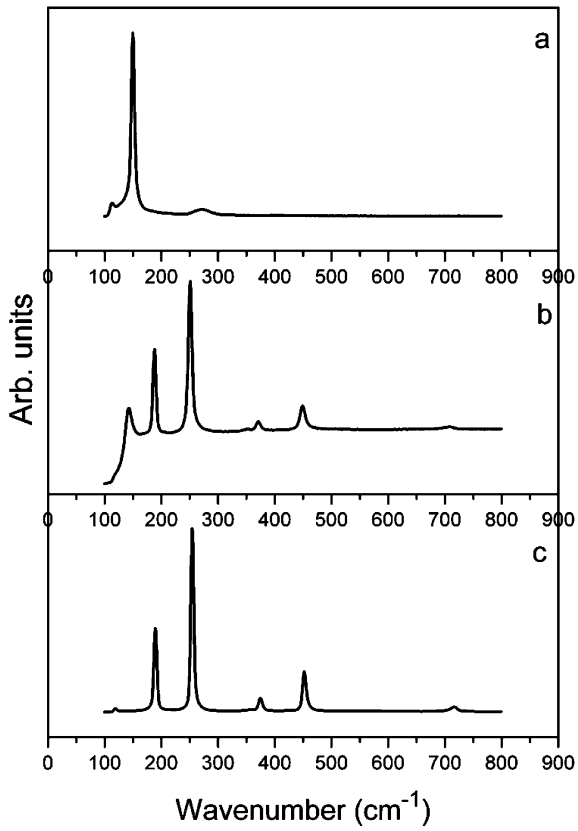

Figure 3. Raman spectra obtained for (a) a pure Sb coating, (b) an Sb/Sb_2O_3 coating, and (c) Sb_2O_3 precipitated from the electrolyte by additions of NaOH.

comparison of Figures 2c and 2b, however, clearly shows that the electrodeposited coating obtained in the absence of HCl did not contain crystalline Sb_2O_3.

Since the XRD pattern in Figure 2b indicated the absence of crystalline Sb_2O_3 in the coatings, the deposits were further studied using Raman spectroscopy. Figure 3 shows Raman spectra recorded for the deposits obtained in the presence and absence of HCl, as well as for the Sb_2O_3 precipitate formed upon the addition of sodium hydroxide. The two peaks at 114 and 149 cm^{-1} and the broad feature at 270 cm^{-1} seen in Figure 3a are characteristic for antimony.[36] The spectrum for the deposit obtained in the absence of HCl, seen in Figure 3b, exhibits the Sb peak at 149 cm^{-1} in addition to peaks which can be ascribed to Sb_2O_3 (see Figure 3c). This shows that the deposit obtained in the absence of HCl did contain both Sb and Sb_2O_3. The spectra in Figure 3b is, incidentally, in good agreement with that reported for Sb_2O_3 nanoparticles containing metallic antimony.[37]

Additional evidence for a mixture of Sb and Sb_2O_3 in the coatings prepared in the absence of HCl is provided by the results of an XPS study of the deposits. The Sb 3d XPS spectra for the deposit prepared in the presence and absence of HCl are shown in Figures 4a and b, respectively. Both spectra clearly show that two antimony oxidation states were present in the deposits. Sb(III) peaks at 540.0 and 530.6 eV

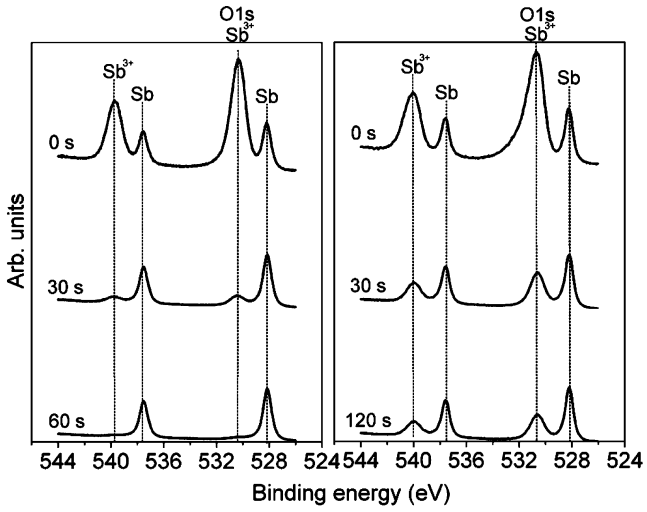

Figure 4. XPS spectra obtained for (a) a pure Sb coating and (b) a Sb/Sb_2O_3 coating. The spectra were recorded before and after sputtering for 30 and 60 s, respectively.

as well as elemental Sb peaks at 537.5 and 528.2 eV are thus seen due to the presence of both Sb_2O_3 and metallic antimony in the deposits. These assignments are in good agreement with previous results reported in the literature.[37,38] It is thus clear that both types of deposits contained Sb_2O_3, at least on the surface. To study if the oxide was present also below the surface, a depth profile was made by analyzing the surface by XPS after a set of sputtering periods. In Figure 4, it is seen that the intensity for the Sb(III) XPS peaks for the pH 1.3 deposit decreased dramatically after a 30 s sputtering period while the corresponding peaks for the deposit obtained in the absence of HCl exhibited high intensities even after sputtering for 120 s. Although a quantification of the amount of oxide in the deposit is complicated by the fact that the O 1s peak and the Sb $3d_{5/2}$ peak at 530.6 eV overlap, it is immediately clear that the deposit prepared in the absence of HCl had a larger oxide content compared to the deposit obtained in the presence of HCl. More importantly, the XPS results indicate that Sb_2O_3 was present within the bulk of the deposit prepared in the absence of HCl, suggesting a continuous co-deposition of Sb_2O_3 throughout the deposition period. The presence of such a continuous co-deposition of Sb and Sb_2O_3 is also in good agreement with the results of our electrochemical quartz crystal microbalance (EQCM) deposition experiments. In the latter experiments, a constant slope of the frequency vs time plot was obtained during electrodeposition in the absence of HCl, except during the first 10 s where the shape of the chronopotentiograms showed that the nucleation of the deposit was taking place. An evaluation of the slope of the frequency vs time plot, however, showed that the slope was too large in comparison with the expected slope for Sb deposition at 100% current efficiency. This too large slope constitutes additional evidence for a continuous coprecipitation of Sb_2O_3 in the absence of HCl throughout the deposition. It should be mentioned that the slopes of the frequency vs time plots obtained in the presence of HCl were in good agreement with the expected value for pure Sb

(36) Lannin, J. S.; Calleja, J. M.; Cardona, M. *Phys. Rev. B* **1975**, *12*, 585.
(37) Zeng, D. W.; Xie, C. S.; Zhu, B. L.; Song, W. L. *Mater. Lett.* **2004**, *58*, 312.
(38) Izquierdo, R.; Sacher, E.; Yelon, A. *Appl. Surf. Sci.* **1989**, *40*, 175.

electrodeposition. A thin layer of Sb_2O_3 is, however, expected to form on the surfaces of the pure Sb coatings as a result of their exposure to oxygen (see Figure 4a). The electrodeposited coatings were also analyzed for carbon as carbon could be incorporated in the coatings during the reduction of the antimony tartrate. No significant amounts of carbon were, however, found in the coatings.

As is depicted in Figure 5, TEM micrographs showed that the coatings contained Sb and Sb_2O_3 nanoparticles with a particle size down to about 20 nm (see Figure 5a) in accordance with the XRD data. The Sb nanoparticles (i.e., the larger and darker particles in Figure 5b) were found to be surrounded by a matrix of smaller Sb_2O_3 particles and the electron diffraction pattern exhibited nanocrystalline Sb_2O_3 rings and a polycrystalline Sb pattern. Since the TEM investigations were performed on powders scratched off from the deposited Sb_2O_3/Sb coatings in air, it is expected that the Sb nanoparticles should be coated with a layer of Sb_2O_3 due to oxidation by oxygen. Small Sb particles could therefore have been completely oxidized to Sb_2O_3, which makes it difficult to estimate the amount of the Sb_2O_3 and Sb nanoparticles in the deposited coatings from the TEM micrographs. As is seen in Figure 5c, there was also evidence for the presence of very small (<2 nm) nanoparticles agglomerated onto the surface of larger particles.

3.2. Electrodeposition Reactions. The present findings clearly show that coatings with different composition and morphology are obtained in the two electrolytes. At pH 1.3 (i.e., in the presence of 0.11 M HCl) deposits composed of relatively large crystals of Sb were obtained while mixtures of Sb and Sb_2O_3 were found after deposition in the absence of HCl. The presence of Sb_2O_3 in the latter deposits, which were composed of nanoparticles, can be explained by a local increase in the pH as a result of the protonation of the tartrate liberated during the reduction of an antimony tartrate complex. Although the exact nature of this complex remains unknown, it is clear that the dimer $Sb_2(H_{-2}L)_2^{2-}$ is a very likely candidate. The latter complex will therefore be used in the reactions below:

$$Sb_2(H_{-2}L)_2^{2-} + 6e^- \leftrightarrow 2Sb + 2H_{-2}L^{4-} \quad (2)$$

$$2H_{-2}L^{4-} + 4H^+ \leftrightarrow 2L^{2-} \quad (3)$$

$$Sb_2(H_{-2}L)_2^{2-} + 4H^+ + 6e^- \leftrightarrow 2Sb + 2L^{2-} \quad (4)$$

In the reactions above $H_{-2}L^{4-}$ denotes the fully deprotonated form of tartaric acid ($^-OOC-CH(O^-)-CH(O^-)-COO^-$) in which both the two carboxylic groups and the two hydroxyl groups have lost their protons. Upon the liberation of the tartrate from the complex, the tartrate OH protons are, however, restored to yield L^{2-} (i.e., $^-OOC-CH(OH)-CH(OH)-COO^-$) according to reaction (3) since L^{2-} should predominate at pH values above 4.37[39] (i.e., $pK_{a,2}$ for the carboxyl groups of tartaric acid). It should be mentioned that the pK_a values for the hydroxyl protons are very high compared to the pH values likely to be attained in the present experiments. From reaction (4), which was obtained by combining reactions (2) and (3), it is clear that protons are consumed in the reduction of the antimony tartrate. As in the analogous copper(II) tartrate, lactate, and citrate systems,[22−25] the magnitude of this local pH increase depends on the buffer capacity of the electrolyte, as well as the current density used. In the electrolyte containing 0.11 M HCl, the pH effect should, however, be negligible for the employed current densities due to the relatively high buffer capacity of this solution. In the absence of HCl, a rapid increase in the pH is, on the other hand, expected due to the poor buffer capacity of the latter electrolyte. With a current density of 1.94 mA/cm^2, approximately 1×10^{-6} mol of H^+ would be consumed per second as a result of reaction (4). Assuming an initial pH of 4.1 in the electrolyte, this consumption can be compared with the total amount of H^+ (within an assumed diffusion layer of a thickness of 180 μm) of about 4×10^{-8} mol. This indicates that the local pH should increase rapidly in the absence of HCl in the electrolyte. To account for the rapid pH increase during the electrodeposition in the absence of HCl, reactions (3) and (4) should in fact rather be written as $2H_{-2}L^{4-} + 4H_2O \leftrightarrow 2L^{2-} + 4OH^-$ and $Sb_2(H_{-2}L)_2^{2-} + 4H_2O + 6e^- \leftrightarrow 2Sb + 2L^{2-} + 4OH^-$, respectively. More importantly, the rapid local pH increase is expected to give rise to the formation of Sb_2O_3 in the vicinity of the working electrode already after a few seconds, according to the following reaction:

$$Sb_2(H_{-2}L)_2^{2-} + 2OH^- + H_2O \leftrightarrow Sb_2O_3 + 2L^{2-} \quad (5)$$

Such a precipitation of Sb_2O_3 is in good agreement with our EQCM findings. Our experimental results also clearly show that Sb_2O_3 can be made to precipitate from the employed electrolyte if the pH is increased to at least pH 6 by additions of sodium hydroxide. This leads us to conclude that some of the precipitated Sb_2O_3 becomes incorporated into the antimony deposits. This model can explain the presence of both Sb and Sb_2O_3 in the deposits obtained in the absence of HCl in the electrolyte as well as in the absence of the oxide in the deposits prepared in the electrolyte containing 0.11 M HCl (in which the precipitation of Sb_2O_3 cannot take place). The rapid increase in the pH in the absence of HCl would also explain the continuous co-deposition of Sb_2O_3, indicated by the XPS and EQCM findings. There is, however, one apparent problem with this hypothesis. The co-deposited Sb_2O_3 should not be stable on the electrode surface during the deposition of antimony as the Sb_2O_3 should be reduced to antimony according to the following reaction:

$$Sb_2O_3 + 6H^+ + 6e^- \leftrightarrow 2Sb + 3H_2O \quad (6)$$

The fact that significant amounts of Sb_2O_3 clearly can be found in the deposits (see Figure 4), however, indicates that reaction (6) is incomplete during the depositions. One explanation for this is that the Sb_2O_3 particles precipitating on the electrode become coated with a growing (protecting) layer of antimony as a result of the combined reduction of the surface layer of Sb_2O_3 and the continuous deposition of Sb from the electrolyte (which carries the constant current).

(39) Harris, D. C. *Quantitative Chemical Analysis*, 6th ed.; W. H. Freeman and Company: New York, 2003.

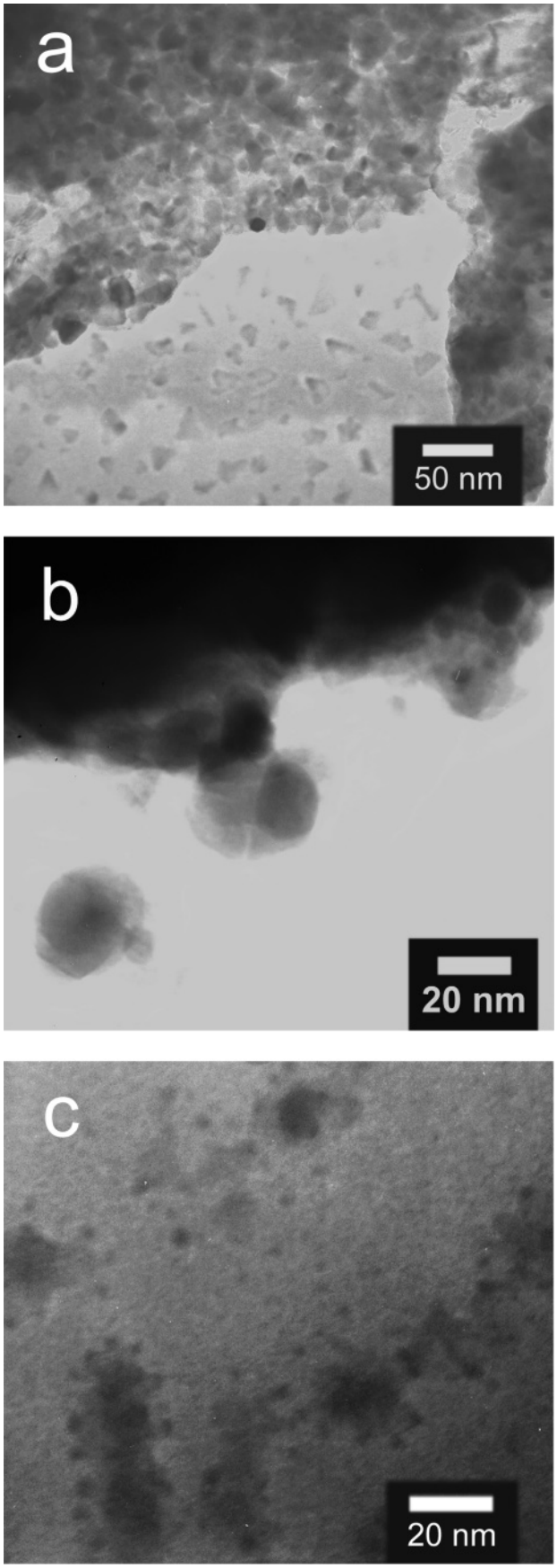

Figure 5. TEM micrographs showing (a) a porous film containing Sb and Sb_2O_3 nanoparticles; (b) larger and darker, slightly faceted nanoparticles of Sb surrounded by a matrix of smaller Sb_2O_3 particles. The electron diffraction pattern exhibited nanocrystalline Sb_2O_3 rings and a polycrystalline Sb pattern; (c) small (<2 nm) nanoparticles agglomerated onto the surface of larger particles.

If the antimony deposition rate is high enough, this can result in an incomplete reduction of the Sb_2O_3 analogous to the situation recently described for the galvanostatic deposition of layers of Cu_2O and Cu.[26] Such a deposition process in which the amount of Sb_2O_3 in the coatings depends on a number of factors such as the current density, pH, buffer capacity of the solution, the hydrodynamic conditions, and concentrations of the antimony tartrate should consequently give rise to a material composed of particles of Sb_2O_3 imbedded in an antimony matrix. The present deposition model also explains the presence of two different Sb crystallite sizes in the Sb/Sb_2O_3 coatings as the smaller crystallites most likely originate from the Sb-coated Sb_2O_3 particles. The presence of the latter particles in the coating is unfortunately difficult to verify using TEM due to the expected oxidation of the Sb layers in contact with oxygen. In the TEM investigations one therefore expects to find a mixture of Sb_2O_3 particles and Sb particles coated with Sb_2O_3, in agreement with the results in Figure 5. The TEM results indicate that the Sb_2O_3 particles are very small which explains the absence of any clear evidence for any Sb_2O_3 XRD peaks in Figure 2. In addition, the presence of smaller Sb crystallites in the Sb/Sb_2O_3 coatings than in the pure Sb coatings suggests that the Sb_2O_3 particles may act as nucleation sites facilitating the deposition of Sb in the form of smaller particles.

Since it is assumed that Sb_2O_3 is co-deposited in the coatings merely as a result of a local increase in the pH during the deposition of antimony, the deposition of the Sb_2O_3 does not involve an electrochemical reaction. This means that the constant current should be due to the deposition of antimony either due to the reduction of antimony tartrate (i.e., reaction (4)) or Sb_2O_3 (i.e., reaction (6)). These two reactions are in fact equivalent with respect to the deposition of antimony as the electron-to-antimony ratio is 1:3 in both reactions (4) and (6). Our experimental results indeed indicate a close to 100% current efficiency during the electrodeposition step since the deposited mass of the pure Sb deposits (i.e., 0.51 mg for an area of 3.14 cm^2) was found to be in good agreement with the corresponding theoretical mass (i.e., 0.53 mg), calculated for a current density of 4.0 mA/cm^2 and a deposition time of 100 s. This current efficiency of about 96% demonstrates the absence of a significant influence of possible side reactions such as reduction of oxygen or hydrogen evolution. The mass of the corresponding deposits prepared in the absence of HCl using the acetone-rinsed nickel substrates was typically 0.39 mg (for an area of 3.14 cm^2). The latter mass is significantly higher that the theoretical mass of 0.31 mg calculated for a pure Sb coating deposited with the same current density and the same deposition time (i.e., 1.94 mA/cm^2 for 120 s), indicating the presence of an additional component in the coatings (i.e., 0.08 mg of Sb_2O_3). These masses indicate the presence of approximately 21% of electroless co-deposited Sb_2O_3 in the coatings. This value is in good agreement with the results of our EQCM measurements, performed during the electrodeposition in the absence of HCl using a current density of 1.94 mA/cm^2, which indicate the presence of 24% of Sb_2O_3 in the corresponding coatings.

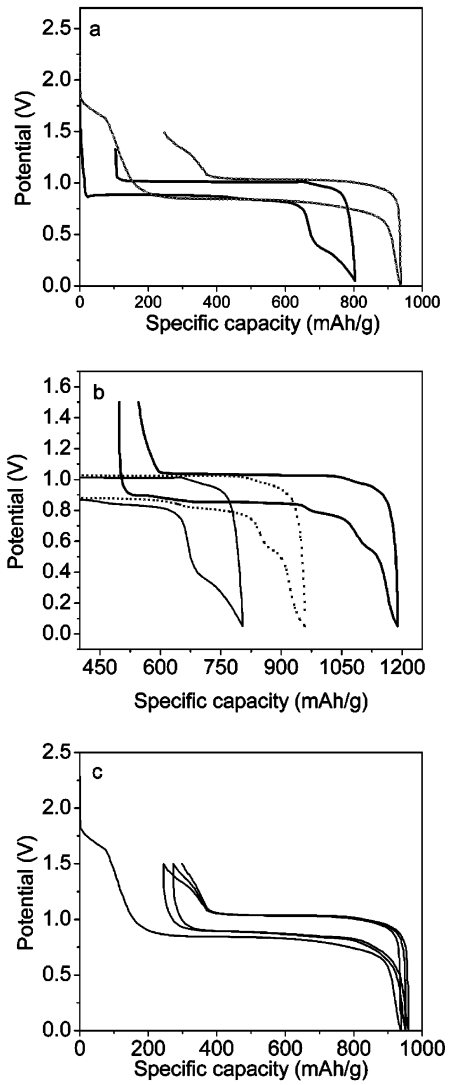

Figure 6. Chronopotentiograms, recorded at a rate of C/10, showing (a) the first cycle for a pure Sb (solid line) and an Sb/Sb$_2$O$_3$ (dotted line) coating, respectively; (b) the first (solid line), second (dotted line), and the tenth cycle (solid line) for the pure Sb coating and (c) the first three cycles for the Sb/Sb$_2$O$_3$ coating.

3.3. Electrochemical Performance of the Coatings as Li-Ion Battery Anodes. As is seen in Figure 6a, which shows the first chronopotentiometric cycle obtained with an Sb and Sb/Sb$_2$O$_3$ deposit, respectively, the cycling behavior of the two types of coatings differed both at potentials around 1.6 and 0.4 V vs Li$^+$/Li. No significant difference in the electrochemical behavior was, on the other hand, seen between the electrochemical behavior of the coatings deposited in the absence of HCl using Ni substrates cleaned in acetone or etched with HNO$_3$. During the first cycle of the Sb/Sb$_2$O$_3$ deposit, a plateau is seen at a potential of around 1.6 V vs Li$^+$/Li. This feature, which is absent for the Sb coating, stems from the reduction of Sb$_2$O$_3$ yielding Sb and Li$_2$O[40,41] according to reaction (7) below:

$$6Li^+ + Sb_2O_3 + 6e^- \leftrightarrow 3Li_2O + 2Sb \qquad (7)$$

Reaction (7) is in fact analogous to the reactions previously described for tin oxide[42,43] as well as many 3d-metal (Co, Ni, Fe, Cu, and Mn)-based oxides.[15,44] Since the EQCM and XPS data suggest that the Sb/Sb$_2$O$_3$ coating is homogeneous with respect to the concentration of Sb$_2$O$_3$, it is reasonable to assume that reaction (7) results in the formation of a material composed of Li$_2$O within a matrix of Sb. In principle, reaction (7) offers an alternative way of estimating the amount of Sb$_2$O$_3$ within the coating. Based on the charge required for reaction (7), the mass of the Sb$_2$O$_3$ within the coating was calculated to be 0.15 mg, assuming that the latter reaction was the only reduction taking place at potentials above approximately 0.8 V. This mass is, however, in poor agreement with the expected Sb$_2$O$_3$ mass of about 0.08 mg. It is therefore clear that reaction (7) cannot be the only reaction taking place at potentials higher than 0.8 V. To explain the experimental results, we consequently need to take at least one additional reaction into account in this potential region. As it is known that a solid electrolyte interface (SEI) can be expected to take place at potentials close to 0.8 V,[45−47] the additional reduction process could involve the formation of such a SEI layer. This is, however, unlikely as a corresponding SEI layer would be expected to form also on the Sb coating. The small charge needed to reach about 0.8 V in Figure 6a for the pure Sb deposit is most likely due to the presence of a thin layer of Sb$_2$O$_3$ on the Sb coating, as indicated by the XPS data in Figure 4a. As will be discussed in more detail below, our data do in fact demonstrate that SEI layers are formed on both types of coatings once the plateau at approximately 0.8 V has been reached. A more likely explanation for the too large charge obtained for the Sb$_2$O$_3$-containing sample at potentials larger than about 0.8 V is that reaction (1), i.e., $3Li^+ + 3e^- + Sb \leftrightarrow Li_3Sb$ (which explains the plateau seen at about 0.8 V for both types of deposits in Figure 6a) starts to contribute to the current well before the latter plateau is reached. A similar phenomenon was incidentally recently reported for some isostructural MSb$_2$O$_6$ (M = Cu, Ni, Co) trirutile-type phases synthesized by Larcher et al.[48] In our case, this mixed reaction effect is not surprising since according to our electrodeposition model, the reduction of Sb$_2$O$_3$ results in the formation of a growing layer of Sb on the remaining Sb$_2$O$_3$ particles. Under controlled current conditions, this means that an increasing fraction of the current has to be taken care of by reaction (1) once the reduction of the Sb$_2$O$_3$ has been initiated. In the chronopotentiogram this can be seen as a gradual shift in the potential toward lower potentials until the potential finally becomes entirely determined by reaction (7). The fact that a too large Sb$_2$O$_3$ mass was obtained above can then be explained by the fact that the

(40) Wang, J.; Raistrick, I. D.; Huggins, R. A. *J. Electrochem. Soc.* **1986**, *133*, 457.
(41) Li, H.; Huang, X.; Chen, L. *Solid State Ionics* **1999**, *123*, 189.
(42) Courtney, I. A.; Dahn, J. R. *J. Electrochem. Soc.* **1997**, *144*, 2045.
(43) Liu, W.; Huang, X.; Wang, Z.; Li, H.; Chen, L. *J. Electrochem. Soc.* **1998**, *145*, 59.
(44) Poizot, P.; Laruelle, S.; Grugeon, S.; Dupont, L.; Tarascon, J.-M. *Ionics* **2001**, *6*, 321.
(45) Peled, E.; Tow, D. B.; Melman, A.; Gerenrot, E.; Lavi, Y.; Rosenberg, Y. *Proc. Electrochem. Soc.* **1994**, *94-4*, 177.
(46) Chusid, O.; Ely, Y. E.; Aurbach, D.; Babai, M.; Carmeli, Y. *J. Power Sources* **1993**, *43*, 47.
(47) Winter, M.; Besenhard, J. O.; Spahr, M. E.; Novak, P. *Adv. Mater.* **1998**, *10*, 725.
(48) Larcher, D.; Prakash, A. S.; Laffont, L.; Womes, M.; Jumas, J. C.; Olivier-Fourcade, J.; Hedge, M. S.; Tarascon, J.-M. *J. Electrochem. Soc.* **2006**, *153*, A1778.

reduction of Sb_2O_3 to Li_3Sb involves 12 electrons/mol of Sb_2O_3 (see reaction (8)) whereas the reduction of Sb_2O_3 to Sb involves only 6 electrons/mol of Sb_2O_3.

$$Sb_2O_3 + 12Li^+ + 12e^- \leftrightarrow 3Li_2O + 2Li_3Sb \qquad (8)$$

The main difference between the two types of anode materials after the initial reduction of the co-deposited Sb_2O_3 (according to reaction (7)) should be the presence of Li_2O in the material deposited in the absence of HCl. However, as this Li_2O is unlikely to be reduced during the chronopotentiometric cycling of the deposits, one should expect that the cycling of the two types of materials should be quite similar once reaction (7) has taken place. As is clearly seen in Figure 6a, this is, however, not the case. A small plateau is thus seen at a potential of about 0.4 V vs Li^+/Li for the Sb coating but not for the obtained Sb/Li_2O coating. This plateau was also absent when using Sb/Sb_2O_3 (i.e., Sb/Li_2O) coatings deposited on etched Ni substrates. In Figure 6b, it is seen that although the plateau at about 0.4 V vs Li^+/Li becomes less pronounced upon repeated cycling of the Sb coating, it can still be observed after ten cycles. The shift to higher specific capacities seen in Figure 6b is due to the fact that the oxidation charge is smaller than the reduction charge on each cycle (see below). Even though the reasons for the appearance of the 0.4 V vs Li^+/Li plateau are not completely understood at present, the data clearly demonstrate that the electrochemical behavior of the Sb and Sb/Li_2O coatings differ significantly in the potential region of interest here. It is also clear that the 0.4 V vs Li^+/Li plateau is unlikely to be due to SEI formation since such a reaction is expected to take place also on the Sb/Li_2O coatings. In this context it is interesting to note that Pralong et al.[19] did not find a corresponding plateau for their Sb coatings prepared by pulsed laser deposition. Since a plateau is seen for the Sb coating in Figure 6a while no such plateau was seen for the Sb coatings prepared by Pralong et al.,[19] it is possible that the different behavior is caused by differences in the morphology of the Sb coatings. Such an effect could also explain the different results for our electrodeposited Sb coatings in the presence and absence of co-deposited Sb_2O_3 as Figure 1 clearly shows that the particle size is significantly different for these coatings. The differences between the Sb and Sb/Li_2O coatings in this potential region may then be due to problems associated with a complete lithiation of the Sb present in the larger particles. The growing layer of Li_3Sb on the Sb particles could give rise to an increasing overpotential causing the potential to drift toward lower potentials. The influence of this effect should become smaller as the Sb particle size is decreased, which could explain the different shape of the chronopotentiogram for the coating prepared in the absence of HCl. As is seen in Figure 6b, the plateau at about 0.4 V becomes less pronounced upon repetitive cycling. One explanation for this could be that the particle size is decreasing during the cycling as a result of the dramatic changes in the volume associated with the lithiation/delithiation processes. The differences seen in Figure 6a, could, however, also be caused by other structural differences between the deposits, or less likely, by a previously unidentified lithiation reaction. These issues call for additional investigations and will therefore be addressed in more detail in a separate communication.

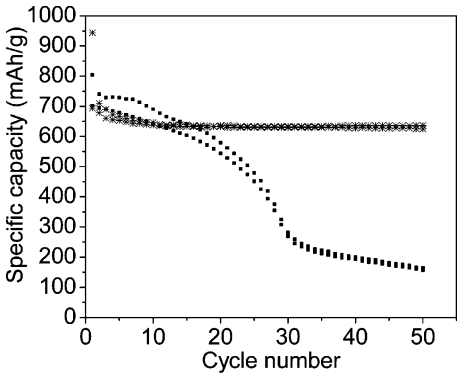

Figure 7. Specific capacities at a rate of C/10 for a pure Sb (squares) and a Sb/Sb_2O_3 (stars) coating, respectively.

As is seen in Figure 6a, the electrochemical behavior of the coatings also differs when the materials undergo oxidation. While the oxidation of the Li_3Sb coating (i.e., reaction (1) reversed) rapidly reaches a constant potential, which is maintained until the potential rapidly drifts away to reach the cutoff potential of 1.5 V, the corresponding curve for the Li_3Sb/Li_2O coating shows a gradual increase in the potential before the cutoff potential is finally reached. The latter effect, which is more clearly seen in Figure 6c, suggests that an increasing potential is needed to maintain the current as a result of a decreasing rate of the oxidation of Li_3Sb to Sb. As the delithiation process should start at the surface and proceed toward the center of the particles, the gradual increase in the potential seen for the Li_3Sb/Li_2O coating could be due to Sb formed on the surface of the particle undergoing oxidation to Sb_2O_3 (i.e., reaction (7) reversed) even though Li_3Sb is still present within the particles. This effect, which clearly should be absent in the absence of Li_2O in the coatings, is very interesting as it suggests that it is possible to regain some of the capacity thought to be irreversibly lost on the first cycle as a result of reaction (7). Evidence for a reoxidation of the reduced metal or a back formation of Sb-based oxides at 1.4 V was in fact also found by Larcher et al.[48] when studying the lithiation and delithiation of $NiSb_2O_6$ and $CoSb_2O_6$ materials. The slight shift of the curves toward higher capacities for the Sb/Li_2O coating seen in Figure 6c indicates that the oxidation charges, nevertheless, were slightly smaller than the reduction charges. The corresponding capacity shift was, however, much more pronounced for the Sb coating (see Figure 6b). From Figure 6a, it is evident that this was due to an incomplete oxidation of the Li_3Sb. The smaller ratio between the oxidation and reduction charges in this case can be explained by the fact that there is no additional process that can assist in maintaining the current (within the allowed potential window). As a consequence, the mismatch between the oxidation and reduction charges is larger for the Sb than for the Sb/Li_2O coatings. The present data consequently suggest that the rate of the oxidation of Li_3Sb is slower than that of the formation of Li_3Sb (i.e., that the reaction $3Li^+ + 3e^- + Sb \leftrightarrow Li_3Sb$ proceeds faster to the right than to the left). These findings are in good agreement with the results of the corresponding studies of $NiSb_2O_6$ and $CoSb_2O_6$ carried out by Larcher et

al.[48] With use of ^{121}Sb Mössbauer spectroscopy, the latter authors nicely showed that 97% of the Sb(III) in Sb_2O_3 was reduced to mainly Li_3Sb at 0 V vs Li^+/Li while 26% Li_3Sb still could be found in the coating after subsequent oxidation at 3.0 V vs Li^+/Li. As will be described below, the differences between the electrochemical behaviors of the two anode materials seen in Figure 6 give rise to significant differences in the cycling stabilities.

Figure 7 shows the specific capacity as a function of the cycle number for the Sb and Sb/Sb_2O_3 coatings, respectively. It is clearly seen that the cycling stability for the latter coating is significantly better than that for the Sb coating. In these calculations, the masses of the deposits containing both Sb and Sb_2O_3 were used while the theoretical masses were used for the coatings containing only Sb. While the Sb/Sb_2O_3 coating shows a cycling performance with a specific capacity close to the theoretical value (i.e., 660 $mA{\cdot}h{\cdot}g^{-1}$) based on reaction (1) during more than 50 cycles, a rapid loss of performance was seen for the Sb coating. This loss of capacity, which is in agreement with previous results,[40,41] was most likely a result of a loss of an increasing fraction of the coating due to the significant volume changes associated with the formation of Li_3Sb during the cycling. As these volume changes should be present during the cycling of both types of materials studied here, it is, however, not immediately clear why the effects should be much less dramatic for the Sb/Sb_2O_3 coatings. One explanation for this could, however, be that the average particle size was significantly smaller in the latter coating. It is well-known that the reversibility of the lithiation−delithiation process of metal oxide materials is improved when the particle size is decreased.[15,42,47,49] It has also been proposed[42] that enhanced stability is obtained when the reacting particles are allowed to expand in the presence of ductile Li_2O particles. The poor stability of the Sb coatings was not coupled to the reduction reactions taking place at potentials below 0.4 V as experiments showed that cycling to 0.4 V rather than to 0.01 V vs Li^+/Li did not improve the cycling stability for these coatings. This is in good agreement with the conclusion that the loss of capacity is coupled to the formation of Li_3Sb, most of which takes place at higher potentials. The results for the Sb/Sb_2O_3 coatings were not found to depend on the pretreatment of the Ni substrate or the current density (1.94 or 4.0 mA/cm^2) employed. It was likewise evident that it was not possible to increase the stability of the coatings by carrying out the electrodepositions at intermediate pH values (i.e., between 1.3 and 4.1) or with a higher current density (i.e., 40 mA/cm^2). Although SEM investigations on cycled Sb/Sb_2O_3 coatings were found to show the presence of significant cracks in the coatings, the cycling behavior of these coatings were still found to be excellent. The latter suggests that the adhesion of this coating to the electrode was maintained even though the particles underwent large volume changes during the cycling. For the larger Sb particles, deposited in the presence of HCl, the risk of a loss of parts of the coating is most likely significantly higher.

As is seen in Figure 7, the capacity for the Sb/Sb_2O_3 coating was very close to the theoretical capacity calculated based on reaction (1). Such a comparison is, however, not entirely relevant since our coatings contained 20−25% Sb_2O_3 and as our data show that some Sb_2O_3 is actually formed upon the oxidation cycle. For a Sb coating containing 25% of Sb_2O_3, the correct theoretical capacity based on reaction (1) should in fact be 633 rather than 660 $mA{\cdot}h{\cdot}g^{-1}$ if the Sb_2O_3 present in the coating is irreversibly reduced to Sb according to reaction (7). The fact that our experimental capacities are larger than 633 $mA{\cdot}h{\cdot}g^{-1}$ must hence be due to a contribution from (the assumed irreversible) reaction (7), as discussed in conjunction with Figure 6. If one assumes that reaction (7) is reversible, a theoretical capacity of 771 $mA{\cdot}h{\cdot}g^{-1}$ is, however, obtained for a coating containing 25% Sb_2O_3. As our experimentally obtained capacity of about 640 $mA{\cdot}h{\cdot}g^{-1}$ corresponds to approximately 83% of the latter value, it is clear that there is a significant capacity contribution due to the Sb_2O_3 also upon repetitive cycling of these coatings. As was recently suggested by Xue and Fu,[27] very large capacities may consequently be realized for high concentrations of Sb_2O_3 in the coatings. For a coating composed entirely of Sb_2O_3, a theoretical capacity of 1103 $mA{\cdot}h{\cdot}g^{-1}$ is obtained based on reaction (8). It is, however, still not clear if it is possible to attain this value in practice. Xue and Fu[27] reported capacities between 691 and 794 $mA{\cdot}h{\cdot}g^{-1}$ for a pulsed laser deposited Sb_2O_3 coating containing 14 mol % of Sb for which the maximum theoretical capacity should be 1041 $mA{\cdot}h{\cdot}g^{-1}$. The latter experimental capacities thus correspond to 66−76% of the theoretical value, indicating that a significant part of the Sb_2O_3 did not cycle reversibly although the coatings were cycled up to 3.0 V vs Li^+/Li. The corresponding values for our coatings, which only contained between 21 and 24% Sb_2O_3, are 83−85% of the theoretical values (i.e., 753 and 767 $mA{\cdot}h{\cdot}g^{-1}$ for 21% and 24% Sb_2O_3, respectively). This finding, which suggests that our coatings cycled better than the coatings made by Xue and Fu,[27] shows that pure Sb_2O_3 coatings do not necessarily provide higher capacities than coatings containing mixtures of Sb and Sb_2O_3 nanoparticles during repeated cycling.

While our reversible capacity for the Sb/Sb_2O_3 coating in Figure 7 was approximately 86−88% of the theoretical value given above, the first cycle capacity (i.e., 934 $mA{\cdot}h{\cdot}g^{-1}$) clearly exceeds the theoretical value by 167 (for 24% Sb_2O_3) and 181 (for 21% Sb_2O_3) $mA{\cdot}h{\cdot}g^{-1}$, respectively. Analogously, the first cycle capacity (i.e., 803 $mA{\cdot}h{\cdot}g^{-1}$) for the pure Sb coating was significantly higher than the 660 $mA{\cdot}h{\cdot}g^{-1}$ expected based on reaction (1). This shows that at least one additional reaction must take place on the first cycle for both types of coatings. A calculation of the excess charges reveals that the extra charge was 0.065 to 0.071 and 0.073 $mA{\cdot}h$ for the Sb/Sb_2O_3 and pure Sb coatings, respectively. In other words, the extra charge was found to be very similar for both coatings. It is therefore reasonable to assume that this extra charge originates from the same reaction(s) in both cases. Based on Figure 6, we may also conclude that the unidentified reaction(s) takes place on the 0.8 V plateau, i.e., simultaneously with reaction (1). A close

(49) Yang, J.; Winter, M.; Besenhard, J. O. *Solid State Ionics* **1990**, *40−41*, 525.

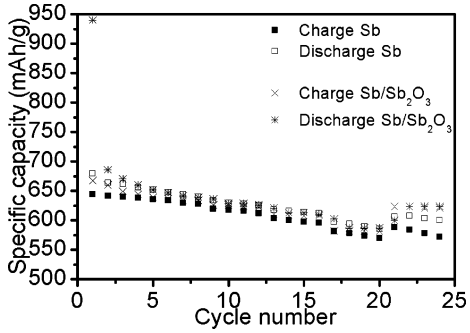

Figure 8. Rate capability of a pure Sb coating and an Sb/Sb_2O_3 coating. In these tests galvanostatic cycling between 1.5 and 0.01 V vs Li^+/Li was performed at four different rates: C/10 for eight cycles followed by C/6 for four cycles; C/3 for four cycles; C for four cycles; and finally C/10 for four cycles.

look at Figure 6c shows that the shape of the first chronopotentiometric curve differs from those of the subsequent cycles. Since it has been reported that an SEI layer can be expected to form at potentials close to 0.8 V,[45−47] our conclusion is that an SEI layer is formed on both coatings on the first cycle as a result of electrolyte degradation reactions. By employing mass spectrometry, Gireaud et al.[50] elegantly showed that significant electrolyte degradation takes place on CoO nanocomposite materials which behave similarly to the coatings investigated here. The fact that our first cycle extra charge was very similar for the Sb and Sb/Sb_2O_3 coatings indicates that the thickness of the obtained SEI layer was very similar in both cases.

Rate capability tests were also performed with the two types of coatings, as is depicted in Figure 8. In these tests, galvanostatic cycling between 1.5 and 0.01 V vs Li^+/Li was performed at four different rates: C/10 for eight cycles followed by C/6 for four cycles; C/3 for four cycles; C for four cycles; and finally C/10 for four cycles. It is seen that the specific capacities for both the pure Sb and the Sb/Sb_2O_3 coatings decrease when the rate is increased and that the overall decrease was approximately 8% when the rate was changed from C/10 to C. When the C/10 rate was resumed after the use of a rate of C, the Sb/Sb_2O_3 electrode exhibited a specific capacity of 624 $mA{\cdot}h{\cdot}g^{-1}$, which should be compared to the value of 640 $mA{\cdot}h{\cdot}g^{-1}$ obtained after ten cycles at a rate of C/10. With the Sb electrode, the corresponding values were 601 and 640 $mA{\cdot}h{\cdot}g^{-1}$. These results thus indicate that the capacity loss upon an increase of the cycling rate was smaller for the Sb/Sb_2O_3 coatings than for the pure Sb coatings. We ascribe this to the presence of nanoparticles in the former coatings.

(50) Gireaud, L.; Grugeon, S.; Pilard, S.; Guenot, P.; Tarascon, J.-M.; Laruelle, S. *Anal. Chem.* **2006**, *78*, 3688.

4. Conclusions

It has been shown that coatings composed of nanoparticles of Sb and Sb_2O_3 can be electrodeposited during galvanostatic reduction of antimony tartrate as a result of the local increase in the pH associated with the protonation of the released tartrate. This pH increase, which is analogous to that previously described for the reduction of copper tartrate, lactate, or citrate complexes, causes precipitation of Sb_2O_3, which becomes embedded in the coating. The expected reduction of the co-deposited Sb_2O_3 is incomplete under galvanostatic conditions due to the formation of a growing layer of Sb on top of the remaining Sb_2O_3. The described procedure, which most likely can be applied also to the manufacturing of other metal−metal oxide systems, constitutes a novel way of manufacturing coatings containing very small Sb and Sb_2O_3 particles. Our results clearly show that such coatings function well as anode materials for Li-ion batteries and that the theoretical capacities for such coatings range from 660 to 1103 $mA{\cdot}h{\cdot}g^{-1}$ depending on the content of Sb_2O_3 in the coating. For a coating containing about 25% Sb_2O_3, as the coatings obtained in this work, the theoretical capacity is 770 $mA{\cdot}h{\cdot}g^{-1}$. The reversible capacities of about 640 $mA{\cdot}h{\cdot}g^{-1}$ experimentally obtained for the deposited Sb/Sb_2O_3 coatings demonstrate that a significant fraction of the Sb_2O_3 cycled reversibly. During the first reduction cycle, the incorporated Sb_2O_3 is reduced to Sb at about 0.8 V vs Li^+/Li which results in the formation of Li_2O nanoparticles within a matrix of Sb analogous to previous results for other metal oxides. Evidence for the formation of a SEI layer of approximately the same thickness was found for both the pure Sb and the Sb/Sb_2O_3 coatings at approximately 0.8 V vs Li^+/Li. It is concluded that the high capacities obtained are due to the presence of the Sb and Sb_2O_3 nanoparticles that facilitate the lithiation and delithiation processes. The good stability also observed for the Sb/Sb_2O_3 coatings demonstrates that the problems associated with the large volume changes during the cycling do not necessarily prevent Sb-containing coatings from being used as anodes in Li-ion batteries. We believe that electrodeposition is a very promising, straightforward, and inexpensive way to manufacture such nanoparticle-based battery materials.

Acknowledgment. The authors thank The Swedish Research Council (Grant 621-2003-3626 and Grant 2005-3356), The Göran Gustafsson Foundation, and The Carl Trygger Foundation for financial support. H.B. also thanks Ångpanneföreningen for additional support. The authors likewise thank Mikael Ottosson for help with the interpretation of the XRD data and Professor Josh Thomas for rewarding scientific discussions.

CM0624769